remote sensing

MDPI

Article

Estimation of Water Stress in Grapevines Using Proximal and Remote Sensing Methods †

Alessandro Matese [1,*], Rita Baraldi [2], Andrea Berton [3], Carla Cesaraccio [4], Salvatore Filippo Di Gennaro [1], Pierpaolo Duce [4], Osvaldo Facini [2], Massimiliano Giuseppe Mameli [5], Alessandra Piga [4] and Alessandro Zaldei [1]

1 Institute of Biometeorology (IBIMET), National Research Council (CNR), Via Caproni 8, 50145 Florence, Italy; f.digennaro@ibimet.cnr.it (S.F.D.G.); a.zaldei@ibimet.cnr.it (A.Z.)
2 Institute of Biometeorology (IBIMET), National Research Council (CNR), Via P.Gobetti, 101, 40129 Bologna, Italy; r.baraldi@ibimet.cnr.it (R.B.); o.facini@ibimet.cnr.it (O.F.)
3 Institute of Clinical Physiology (IFC), National Research Council (CNR), Via Moruzzi 1, 56124 Pisa, Italy; andrea.berton@ifc.cnr.it
4 Institute of Biometeorology (IBIMET), National Research Council (CNR), Traversa La Crucca, 3, 07100 Sassari, Italy; c.cesaraccio@ibimet.cnr.it (C.C.); p.duce@ibimet.cnr.it (P.D.); a.piga@ibimet.cnr.it (A.P.)
5 AGRIS Sardegna, Loc. Bonassai S.S. 291 Sassari-Fertilia—Km. 18,600, 07100 Sassari, Italy; mgmameli@agrisricerca.it
* Correspondence: a.matese@ibimet.cnr.it; Tel.: +39-055-303-3711
† This paper is an extended version of our paper published in Acta Horticulturae 2017—International Symposium on Sensing Plant Water Status—Methods and Applications in Horticultural Science.

Received: 6 December 2017; Accepted: 12 January 2018; Published: 16 January 2018

Abstract: In light of climate change and its impacts on plant physiology, optimizing water usage and improving irrigation practices play a crucial role in crop management. In recent years, new optical remote sensing techniques have become widespread since they allow a non-invasive evaluation of plant water stress dynamics in a timely manner. Unmanned aerial vehicles (UAV) currently represent one of the most advanced platforms for remote sensing applications. In this study, remote and proximal sensing measurements were compared with plant physiological variables, with the aim of testing innovative services and support systems to farmers for optimizing irrigation practices and scheduling. The experiment, conducted in two vineyards located in Sardinia, Italy, consisted of two regulated deficit irrigation (RDI) treatments and two reference treatments maintained under stress and well-watered conditions. Indicators of crop water status (Crop Water Stress Index—CWSI—and linear thermal index) were calculated from UAV images and ground infrared thermal images and then related to physiological measurements. The CWSI values for moderate water deficit (RDI-1) were 0.72, 0.28 and 0.43 for 'Vermentino', 'Cabernet' and 'Cagnulari' respectively, while for severe (RDI-2) water deficit the values were 0.90, 0.34 and 0.51. The highest differences for net photosynthetic rate (Pn) and stomatal conductance (Gs) between RDI-1 and RDI-2 were observed in 'Vermentino'. The highest significant correlations were found between CWSI with Pn ($R = -0.80$), with Φ_{PSII} ($R = -0.49$) and with Fv'/Fm' ($R = -0.48$) on 'Cagnulari', while a unique significant correlation between CWSI and non-photochemical quenching (NPQ) ($R = 0.47$) was found on 'Vermentino'. Pn, as well as the efficiency of light use by the photosystem II (PSII), declined under stress conditions and when CWSI values increased. Under the experimental water stress conditions, grapevines were able to recover their efficiency during the night, activating a photosynthetic protection mechanism such as thermal energy dissipation (NPQ) to prevent irreversible damage to the photosystem. The results presented here demonstrate that CWSI values derived from remote and proximal sensors could be valuable indicators for the assessment of the spatial variability of crop water status in Mediterranean vineyards.

Keywords: unmanned aerial vehicle (UAV); grapevine; crop water stress index (CWSI); stem water potential (SWP); photosynthesis; fluorescence

1. Introduction

Water availability is a critical factor for assessing the impact of climate change on agriculture and agricultural water management. Water demand is increasing and, therefore, an efficient use of water is crucial, especially for agriculture, which is the major sector for the use of freshwater resources. The EU Common Agricultural Policy reports that 44% of the total water withdrawal in Europe is used for agriculture (http://ec.europa.eu/agriculture/envir/water/). High-value crops such as grapevines are very sensitive to water stress and irrigation is increasingly used to improve crop quality performance.

Crop spatial variability can be a factor that may limit irrigation efficiency. Uniform irrigation that does not consider the real water needs of plants frequently may result in a water deficit in some areas while others are waterlogged. In viticulture, water deficits adversely affect different aspects of performance parameters, such as vegetative growth, yield, berry composition and wine sensory compounds [1].

It is well known that even short-term water deficits affect growth processes and induce stomatal closure, which reduces transpiration and, consequently, evaporative cooling, resulting in an increase in leaf temperature. Studies of leaf temperature increase and its correlation with crop water stress have been carried out using thermal infrared thermometers over a period of decades [2]. Jones [3] suggested that greater precision in irrigation management could potentially be obtained using plant-based responses rather than soil water status measurements. However, this monitoring is time-consuming.

To measure plant water status, there are a number of widely used indirect parameters, known to be indicative of water deficits, which can be determined by remote sensing techniques. Remote and proximal sensing images acquired with high resolution thermal cameras, mounted at ground level or on unmanned aerial vehicles (UAV), have spatial resolutions of a few centimeters. They are thus able to provide accurate enough information for both assessing plant water status in the field and implementing appropriate irrigation management strategies [4–7]. The crop water stress index (CWSI), a thermally-derived indicator of water deficit based on leaf/canopy temperature measurements [2] has been used to assess the water status of crops such as grapevines [8], French beans [9], wheat [10], rice [11], maize [12] and cotton [13].

Baluja [14] assessed the water status of a commercial, rain-fed vineyard of 'Tempranillo' by thermal and multispectral imagery using an unmanned aerial vehicle (UAV). Bellvert [15] evaluated the correlation between CWSI and leaf water potential in a 'Pinot Noir' vineyard, reporting that for an accurate CWSI analysis the minimum spatial resolution of images should be 0.3 m pixel^{-1}.

Many studies of plant water stress have analyzed the relationships between air temperature, remote sensing indices, and physiological parameters such as stomatal conductance (Gs) and stem water potential (SWP). Gonzalez-Dugo [16] suggested that the requirements to achieve real-time drought stress monitoring using aerial platforms and to help the farmer's decision-making process are: (i) a strong correlation between stress indices and actual water deficit in the field; (ii) a spatial resolution high enough to enable pure canopy pixels to be targeted, avoiding mixed soil/vegetation pixels; (iii) the evaluation of entire fields in a single flight; and (iv) faster turn-around acquisition and processing times to provide quasi-real-time water status maps.

The images indicate the current plant water status, which changes when irrigation is applied. This actual water status can be useful to characterize spatial variability or to detect leaks and other irrigation system problems. Clearly, multi temporal images represent an excellent tool for change detection, providing much more information on canopy temperature and changes in plant water status within an irrigation cycle than a single image. However, any image acquisition is costly even when using low-cost UAV solutions. Another crucial point to be studied is the frequency of flight acquisition.

In recent years, many relevant advances have also been made in the field of plant water status measurement by near-surface remote sensing techniques, using radiometric instruments or imaging sensors. As an example, various imaging methods became common for the analysis of plant stress responses by automated phenotyping [17]. In addition, several imaging techniques have been developed to detect early signs of stress by monitoring changes in water status, photosynthetic efficiency and the accumulation of secondary metabolites or structural modifications [18–21].

The physiological responses of plants to water deficits are well-known. Plants react to water deficits by several mechanisms that allow adaptation to slow or fast water shortages, paying special attention to CO_2 gain. Stomatal closure and decreases in the mesophyll conductance of CO_2 are among the earliest responses to drought, whereby low CO_2 concentrations in the chloroplast limit photosynthetic C fixation [22]. Under a decreased rate of CO_2 assimilation induced by water stress, light energy absorbed by the leaf cannot be used to drive photosynthetic electron transport (photochemistry) and part of this energy is diverted to other processes to protect the photosynthetic system, increasing the non-photochemical fluorescence quenching [23]. For this reason the chlorophyll fluorescence technique has become a valuable and simple tool to measure the extent of plant tolerance to stress [24–26], providing useful information on energy absorption, utilization and dissipation, and electron transport in the photosystem II (PSII; [27]).

With the perspective of testing innovative services and support systems to farmers for the optimization of irrigation practices and scheduling, in this study remote and proximal sensing measurements were compared with plant physiological variables. The main goals were investigating the potential of digital thermal imaging to reveal different responses of vines to irrigation treatments and improving irrigation management in vineyards.

2. Materials and Methods

2.1. Experimental Sites

The study was conducted during the 2015 growing season in two 1.7-ha vineyards of commercial wineries in Sardinia, Italy. The first experimental site, located near Arzachena in Northeastern Sardinia (41°03′12″N, 9°20′43″E, 115 m above sea level (a.s.l.)), consists of the ancient cultivar 'Vermentino'. The eight-year-old vineyard was planted along a north-northwest to south-southeast row orientation, at a spacing of 2.5 m × 1.0 m, and with a vertical shoot positioning training system. The slope of the experimental field was equal in average to 10% along the West-East direction. The soil is sandy loam, with more than 65% sand. The second experiment, conducted near Usini in Northwestern Sardinia (40°39′26″N, 8°31′16″E, 198 m a.s.l.), includes two cultivars, the rare local grape 'Cagnulari' and the international cultivar 'Cabernet Sauvignon'. The vines were planted in 1995 along a north to south row orientation, at a spacing of 2.4 m × 1.0 m and with a vertical shoot positioning training system. The slope of the field was less than in Arzachena and of about 6% along the row orientation. The soil is clay loam, with about 30% clay.

In our experimental vineyards, the cover fraction ranged from 20% (Usini) to 28% (Arzachena). The typical leaf area index (LAI) development of the studied cultivars in the experimental areas shows a rapid increase until mid-June (LAI approximately equal to 2.2), a maximum value in early August (LAI around 3.2) and a decline until late September (LAI around 2.5).

The climate at both sites is Mediterranean, with warm and dry summers and mild winters. Annual minimum and maximum mean air temperatures occur in January and August, with values of 9.7 °C and 23.6 °C and 8.8 °C and 24.2 °C, at Arzachena and Usini, respectively. Rainfall events occur mainly in autumn, winter and early spring, with a long-term annual average of about 530 mm and 640 mm at Arzachena and Usini, respectively. The dry season may last from May through September, with very low rainfall in total during that period (for example, less than 70 mm during the 2015 season at both sites). In that period, the evaporative demand (expressed as ETo totals) was of 760 mm and 800 mm at Usini and Arzachena, respectively, and the full crop water requirements (ETc) was estimated

as 520 mm and 570 mm, at Usini and Arzachena, respectively. The standard irrigation practices adopted at the two grapevines consist in: (i) an irrigation strategy based on soil water potential thresholds and regulated deficit irrigation management at the Arzachena vineyard, (ii) no irrigation, with supplemental irrigation based on empirical evaluations, at the Usini grapevine field.

The experimental vineyards were irrigated with a semi-automated drip system, with approximately one pressure-compensating emitter per vine (2.0 and 4.0 L h^{-1} at Arzachena and Usini, respectively). Irrigation management consisted of two regulated deficit irrigation (RDI) regimes with two levels of water deficit. Application rates were determined taking into account the readily available soil water in the root zone. Irrigation was applied from the initial stages of fruit growth until grape maturation. In summary, the following irrigation treatments, based on midday SWP measurements, were applied: (i) RDI-1, moderate water deficit, with irrigation water applied when SWP values were lower than −0.9 MPa, and (ii) RDI-2, severe water deficit, with irrigation water applied when SWP values dropped below −1.2 MPa (Table 1). The experiments were performed as a randomized block design and three replicates of each treatment within each block were assigned. Individual plots comprised 210 vines (three rows with seventy plants each), and a total of six plots were monitored. Two additional plots (two rows with seventy plants each) were kept under water deficit or well-watered during the period immediately prior to the UAV flight to have dry (treatment dry) and wet (treatment wet) reference surfaces during the UAV campaigns. For the Arzachena site, the time period between the beginning of the dry treatment and the UAV campaign was 15 days, whereas for Usini, there was no watering throughout the growing season before the UAV campaign. The irrigation management of the rest of the vineyards was scheduled according to the normal farm practices, i.e., irrigation applications were based on RDI-1.

Meteorological data for the entire experimental period were provided by two automated weather stations of the Regional Environmental Protection Agency of Sardinia (ARPAS), located within the experimental vineyards of Arzachena and Usini.

Table 1. Threshold values of midday stem water potential (SWP) by experimental site, treatment, and month. The number of irrigation applications and the total volume of water applied are also reported.

Vineyard	Treatment	May (MPa)	June (MPa)	July (MPa)	August (MPa)	September (MPa)	Irrigation Number (n)	Irrigation Volume (m^3 ha^{-1})
Arzachena	RDI-1	−0.6	−0.9	−0.9	−0.9	−1.4	9	768
	RDI-2	−0.6	−1.2	−1.2	−1.2	−1.4	6	472
Usini	RDI-1	−0.6	−0.9	−0.9	−0.9	−1.4	2	366
	RDI-2	−0.6	−1.2	−1.2	−1.2	−1.4	1	133

2.2. Remote Sensing Measurements

2.2.1. UAV Platform and Payload

Remote aerial surveys were performed using an open-source UAV platform consisting of a modified multi-rotor MikrokopterOktoXL (HiSystems GmbH, Moomerland, Germany). The UAV platform, controlled by an autopilot, was equipped with a global positioning system (GPS) V3.0 module as positioning system, with a 2 kg payload for a 15 min flight time, and a vertical take-off and landing capability. Flight parameter communication to the ground operator was provided by a radio link at 2.4 GHz, with remote sensing data transmission performed at 5.8 GHz. The core of the UAV system is a flight control board, based on an ATMega1284P microcontroller (Atmel Corporation, San Jose, CA, USA), which communicates with the eight brushless controllers by a two-wire bi-directional serial bus (I2C). It integrates a pressure sensor and three-axis accelerometers to calculate and align the UAV with gravity vectors. The flight control board is linked to a navigation control board, equipped with an ARM9 microcontroller (Atmel Corporation, San Jose, CA, USA) and a MicroSD slot card for waypoint data storage. An integrated navigation sensor system (INS) allows various levels of autonomous flight. The INS system is based on a tridimensional (3D) digital compass to monitor the *z* (yaw) axis rotation, and a LEA-6 GPS module (U-blox AG, Thalwil, Switzerland) with a circular error

of about 2 m. The UAV mounts eight ATMega8 control cards (Atmel Corporation, San Jose, CA, USA), dedicated to the management of each brushless motor with a very quick time response (less than 0.5 ms). The flight plan was managed through the Mikrokopter Tool software, which allows a route of waypoints to be generated as a function of the sensor field of view (FOV), the degree of overlap between the images and the ground resolution needed. A universal camera mount equipped with three servomotors allows accurate image acquisition through the compensation of tilt and rolling effects.

A thermal camera (FLIR TAU II 320, FLIR Systems, Inc., Wilsonville, OR, USA) was used for thermal data acquisition. This sensor, optimized for UAV applications, is of minimal size (44.5 mm × 44.5 mm × 30.0 mm) and weight (72 g). When flying at 100 m height, imaging sensor characteristics, i.e., 324 pixels × 256 pixels and 24° × 18° FOV with fixed focal length of 19 mm, allowed to obtain ground level images of about 40 m × 30 m in size, with a resolution of 0.13 m pixel^{-1}. The camera was equipped with an uncooled sensor able to measure long wave radiation in the spectral range 7.5–13 µm. Radiometric calibration was conducted in the laboratory, using a blackbody under varying target and ambient temperatures.

2.2.2. Flight Survey

The UAV flight campaign was conducted in the experimental vineyards on 4–5 August 2015. At both sites, UAV surveys were conducted by flying once at 70 m above ground level at midday, obtaining 0.09 m pixel^{-1} ground image resolution. The camera was set to a fixed exposure with an automatic trigger at 0.2 s frequency. The waypoint route was generated to obtain more than 80% overlap both among photos (forward overlap) and among flight lines (lateral overlap), in order to achieve the highest accuracy in the mosaicking elaboration step. The images were recorded during clear sky conditions.

2.2.3. Remotely-Sensed Data Collection and Processing

Brightness temperature measured by the thermal camera was converted to radiometric temperature assuming a leaf emissivity coefficient of 0.98 as reported by Jones and Vaughan [28]. Leaf radiometric temperature acquired in the thermal infrared spectral region allows computing maps of leaf temperature and, through the estimation of CWSI, of plant water deficit. CWSI was calculated using the equation [29,30]:

$$\mathrm{CWSI} = (\mathrm{Tleaf} - \mathrm{Twet})/(\mathrm{Tdry} - \mathrm{Twet}) \quad (1)$$

where Tdry and Twet represent the temperature of a stressed leaf and of a "wet" leaf in the total absence of stress, respectively, while Tleaf indicates the actual leaf surface radiometric temperature. Tleaf data in the absolute temperature (K) were calculated from the thermal camera digital number (DN) using the empirical line method, as reported by [5]. The DN-values in the thermal imagery represent at-sensor radiance values. Radiometric calibration was done using three different colored panels (1 m × 1 m) at known temperatures as a reference (Table 2).

Table 2. Reference panel temperatures (°C), Twet and Tdry (°C) values for remote and ground procedures at both experimental sites.

	Arzachena	**Usini**
Twet (remote procedure)	23	25
Tdry (remote procedure)	46	43
Twet (ground procedure)	32	27
Tdry (ground procedure)	41	35
White panel	35	32
Blue panel	56	53
Black panel	68	67

Measurements were taken continuously every 10 s during the flight with a hand-held thermal camera (Flir i7, FLIR Systems, Inc., Wilsonville, OR, USA). The procedure for estimating reference temperatures (Tdry and Twet) is crucial for obtaining accurate temperature maps. The adopted methodology was proposed by Jones et al. [28]. The leaves of two vines were coated on both sides with Vaseline to prevent transpiration and stop transpiration cooling, simulating the leaf physiological response to water stress conditions. The wet reference was obtained by wetting both sides of the leaves of another two vines. Tdry and Twet were measured 30 min after applying Vaseline and 20 s after wetting, respectively (Table 2).

The thermal images acquired by UAV were mosaicked using Agisoft Photoscan Professional Edition 1.1.6 (Agisoft LLC, St. Petersburg, Russia). A polygon mesh was computed from the dense 3D point cloud and the pixel values of each image were then projected onto the mesh to create an orthomosaic. When combined with the GPS positions, this process allows the creation of a high-resolution orthophoto and a digital elevation model (DEM) of the experimental site. Two data extraction methods were used: the first for comparing CWSI and SWP values of the four irrigation treatments at the whole vineyard scale, the second for comparing CWSI and chlorophyll fluorescence data in just a few referenced sampling points. The first method allowed us to correctly extract pure canopy pixels from the high resolution UAV thermal imagery, thanks to the exclusion of underlying shadows and soil pixels based on DEM reconstruction of the whole vineyard [31]. All the data extracted by the rows were averaged for each irrigation regime and compared with ground SWP sampling.

The second method consisted of selecting manually pure vine pixels for each vine based on a region of interest (ROI) in the center of each row. Ground sample panels used as reference were placed in front of the sampled vines to facilitate the further extraction of pure pixels.

2.3. Proximal Sensing Measurements

Infrared Thermography and Thermal Indices

Thermal image analysis from the proximal platform was performed to support the results obtained from the UAV and physiological measurements. Grapevine canopy temperature was evaluated using infrared thermography techniques by direct measurements taken during sampling days, for a two-month period, from berries at the pea-size stage until maturation. Infrared images were taken using an infrared thermal imaging camera (InfRec R500Pro, Nippon Avionics Co. Ltd., Tokyo, Japan) with a resolution of 640 × 480 pixels, operating in the 8–14 μm waveband range, and equipped with an red, green and blue (RGB) acquisition imaging system (five megapixels resolution) that adds clear visual images to thermal images. The thermal resolution was 0.03 °C and the accuracy of temperature measurement was less than ±1 °C. Images were taken on sampling days, between 10.00 and 11.00 a.m., at a distance of 1.5 m from the lateral canopy foliage. Infrared images were obtained from three plants per cultivar and treatment for a total of 12 and six plants at the Usini and Arzachena sites, respectively, with three replications for each plant. Canopy emissivity was set at 0.98 as reported by Jones and Vaughan [28]. Visible digital images from the combined RGB acquisition imaging system of the camera were taken simultaneously with infrared measurements to support the subsequent analysis of the thermal images. For each image, a combined approach based on visible and thermal images was then applied to separate leaf and non-leaf material by color discrimination [32] using a specific software (InfReC Analyzer Professional NS9500Pro). To derive stress indices, values of minimum, maximum and mean temperatures, coefficient of variation (CV, %) and temperature range (maximum difference) were calculated for each photo frame inside an ROI of the canopy that included vine leaves. Wet and dry reference temperatures were also calculated on each image within the ROIs of the specific surface, in line with the methodology used by several authors [33,34]. For this, an artificial wet surface, made of cotton cloth and maintained continuously wet with cold water, was used to estimate the reference wet temperature, and thus simulate leaves with fully open stomata. The reference dry temperature was estimated using a black aluminum surface,

5 cm long, 10 cm wide and 0.3 cm thick. This method for obtaining reference temperatures is different but comparable to that reported by several authors [33–35], with the methodology cited in the previous paragraph. The choice of artificial surfaces for measuring reference temperatures was due to the need to obtain data from numerous repetitions, by plant and treatment, quickly and efficiently, in a short time period (10–11 a.m.). The two references were used in conjunction with canopy temperatures to calculate the CWSI values using Equation (1). The linear thermal index (Ig) was also calculated as

$$\text{lg} = (\text{Tdry} - \text{Tcanopy})/(\text{Tcanopy} - \text{Twet}) \quad (2)$$

Data from each cultivar and sampling day were subjected to a one-way variance analysis (XLSTAT, 2015) with two irrigation regimes (moderate and severe water deficit) and nine observations per treatment, using a Tukey's test for mean separation ($p < 0.05$).

2.4. Physiological Measurements

2.4.1. Stem Water Potential

Midday stem water potential (SWP) was assessed on mature shaded leaves, enclosed in bags and covered by aluminum foil for at least 30 min to prevent transpiration and to allow leaves to approach the stem water potential. In each experimental plot, one shaded leaf was sampled on two well-developed and healthy vines located at the end and in the center of the row (six measurements per irrigation regime at each site). SWP was measured twice a week from fruit set (beginning of the irrigation season) until harvest using a pump-up pressure chamber (PMS Instrument Company, Albany, NY, USA).

2.4.2. Leaf Gas Exchange and Fluorescence

Leaf gas exchange (net photosynthesis, Pn and stomatal conductance, Gs) and chlorophyll fluorescence were measured between 10 a.m. and 12 p.m. on two fully-expanded leaves per plant at the same physiological stage (from the eighth to the tenth leaf from the bottom) on three plants per replicate of the different treatments using the LI-6400XT portable photosynthesis system (LI-COR, Lincoln, NE, USA) equipped with 6400-40 leaf chamber fluorometer. Directly after recording the gas exchange data, the maximum fluorescence in the light-adapted state (Fm') was recorded, the actinic light was then turned off and the far red light turned on to measure the minimal fluorescence in a light adapted state (Fo'). The maximum photochemical efficiency of photosystem II (PSII) in dark-adapted leaves (Fv/Fm), maximum efficiency of PSII photochemistry in light-adapted leaves (Fv'/Fm'), the actual photochemical efficiency of PSII (ΦPSII) and non-photochemical quenching (NPQ) were calculated as (Fm − Fo)/Fm, (Fm' − Fo')/Fm', (Fm' − F)/Fm', and Fm − Fm'/Fm', respectively [36]. Measurements were performed between 1 and 2 p.m. at reference CO^2 400 µmol mol^{-1}, PAR (photosynthetic active radiation) 1000 µmol m^{-2} s^{-1}, ambient temperature and a relative humidity of 30–50%. Leaf dark acclimation was induced for 30 min prior to fluorescence measurement using dark-adapting leaf-clips shrouded with aluminum foil to avoid temperature increase [37]. After dark-adaptation, minimal fluorescence (Fo), maximal fluorescence (Fm) and variable fluorescence (Fv = Fm − Fo) were measured automatically under a low modulated light over a 0.8-s period.

3. Results

3.1. Remote Sensing Dataset

The first step of thermal images analysis provided the calculation of the CWSI values for each row using the first data-extraction method. CWSI maps were obtained by an interpolation using a 50 m × 50 m window moving average of CWSI values for the pure canopy pixels (Figure 1). Figure 1 shows the experimental design relative to the irrigation management treatments, overlapped with

the CWSI maps of the two vineyards. Then, the spatial variability of water stress was evaluated. The results related to each irrigation regime are presented in Table 3.

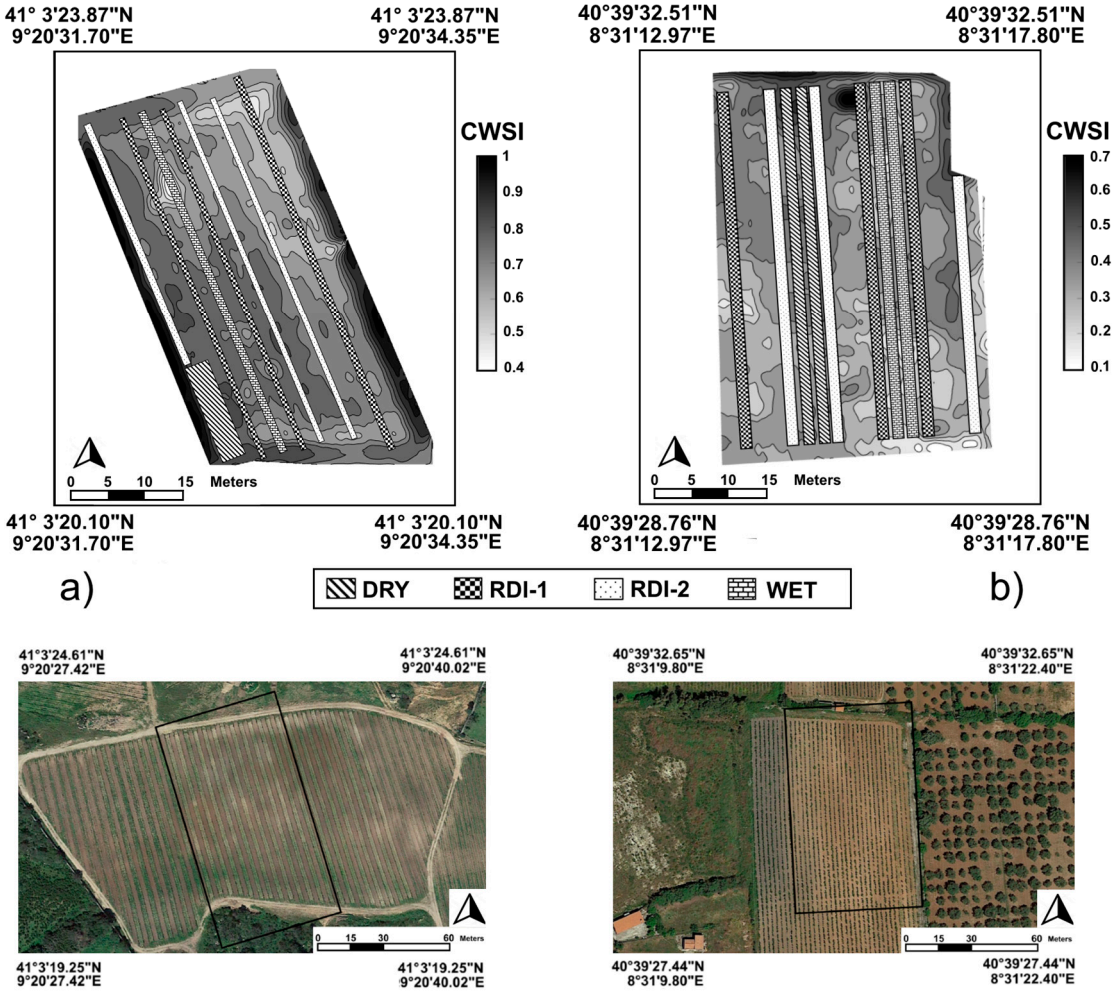

Figure 1. Crop water stress index (CWSI) acquired from Unmanned aerial vehicle (UAV) at Arzachena (**a**) and Usini (**b**) with treatment plots superimposed on the maps.

Table 3. CWSI calculated from UAV images, for 'Vermentino' at Arzachena site and 'Cabernet Sauvignon' and 'Cagnulari' at Usini site under well-irrigated (wet), moderate (RDI-1) and severe (RDI-2) water stress, and dry conditions (dry). Values represent the mean ± standard error (SE). Different letters indicate significant differences between treatments ($p \leq 0.05$) based on one-way analysis of variance (ANOVA) (Tukey test).

	'Vermentino'	'Cabernet'	'Cagnulari'
		CWSI	
Wet	0.77 ± 0.08 a	0.22 ± 0.03 a	0.34 ± 0.04 a
RDI-1	0.72 ± 0.09 a	0.28 ± 0.04 b	0.43 ± 0.05 ab
RDI-2	0.90 ± 0.06 b	0.34 ± 0.05 c	0.51 ± 0.12 b
Dry	0.97 ± 0.03 b	0.47 ± 0.02 d	0.63 ± 0.04 c

At Arzachena, CWSI differences in 'Vermentino' were significant only when higher (wet, RDI-1) and lower (RDI-2, dry) water-availability treatments were compared. At Usini, the CWSI means were significantly different between all treatments of both 'Cabernet' and 'Cagnulari' plants;

only in 'Cagnulari' did the results for RDI-1 not significantly differ from those of the wet and the RDI-2 treatments.

3.2. Proximal Sensing Dataset

CWSI values relative to the moderate and severe water deficit irrigation regimes are shown in Figure 2 by cultivar and site. Regardless of cultivar and site, the CWSI values were always higher under severe rather than under moderate water deficit regimes, in agreement with the results obtained from the UAV flight data, with the largest values observed at the Arzachena site, characterized by more severe drought conditions. At Arzachena, differences between treatments were not significant, except for 5 August (Figure 2a). At Usini, on the contrary, the differences between treatments were clear, as shown by the statistical significance ($p < 0.05$) for both cultivars and sampling days, with the exception of 'Cabernet Sauvignon' on 23 July (Figure 2b,c). In addition, at the Usini experimental site, the differences between the CWSI values of 'Cagnulari' and 'Cabernet Sauvignon' cultivars were small, with mean percentage differences lower under moderate (2–9%) than severe water deficit (12–15%), and with highest values for 'Cagnulari' under severe deficit conditions (Figure 2b,c).

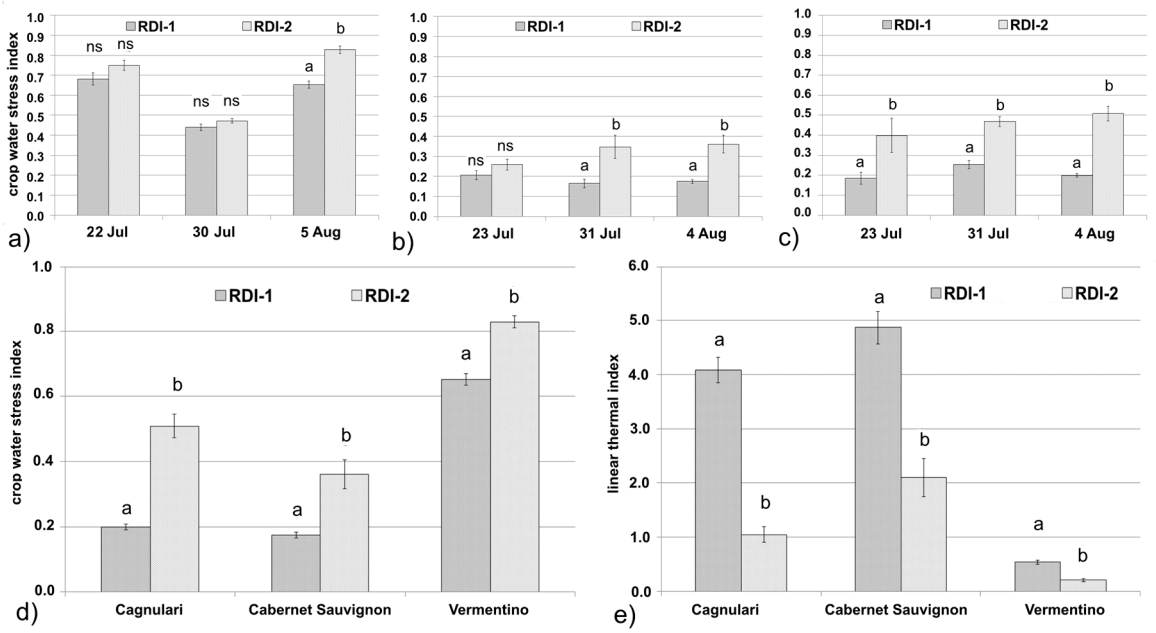

Figure 2. Crop water stress index (CWSI) for (**a**) 'Vermentino' at Arzachena, (**b**) 'Cabernet Sauvignon' at Usini, and (**c**) 'Cagnulari' at Usini, under moderate (RDI-1) and severe (RDI-2) water deficit regimes during three sampling days from berries at pea-size stage until maturation. (**d**) CWSI for all cultivars under moderate and severe water deficit regimes measured on the UAV flight days. (**e**) Linear thermal index (lg) for all cultivars and both sites under moderate and severe water deficit regimes measured on the UAV flight days. Values are means ± SE ($n = 9$). Different letters indicate significant differences between treatments ($p \leq 0.05$) based on one-way ANOVA (Tukey test).

3.3. Physiological Dataset

The SWP values of 'Vermentino' and 'Cagnulari' were not significantly different when wet vs. RDI-1 and RDI-2 vs. dry were compared, while the two groups (wet–RDI-1 and RDI-2–dry) were statistically different from each other, demonstrating that only severe water deficit significantly affected SWP (Table 4). In 'Cabernet Sauvignon' the SWP was statistically different in all treatments, suggesting a greater sensitivity to water availability of this cultivar. In agreement with the remote sensing results, the low values of SWP obtained at Arzachena also for the wet treatment (−0.78) confirmed the combined effect of pedo-morphological and environmental conditions on plant water status.

Table 4. Stem water potential for 'Vermentino' at Arzachena site and 'Cabernet Sauvignon' and 'Cagnulari' at Usini site under well-irrigated (wet), moderate (RDI-1) and severe (RDI-2) water stress and dry conditions (dry). Values represent the mean ± SE. Different letters indicate significant differences between treatments ($p \leq 0.05$) based on one-way ANOVA (Tukey test).

	'Vermentino'	'Cabernet'	'Cagnulari'
		Stem Water Potential (MPa)	
Wet	−0.78 ± 0.03 b	−0.43 ± 0.01 d	−0.54 ± 0.02 b
RDI-1	−0.96 ± 0.05 b	−0.82 ± 0.09 c	−0.71 ± 0.10 b
RDI-2	−1.27 ± 0.03 a	−1.06 ± 0.64 b	−1.13 ± 0.05 a
Dry	−1.34 ± 0.09 a	−1.31 ± 0.03 a	−1.26 ± 0.01 a

At Arzachena, the moderate water reduction RDI-1 did not significantly affect net photosynthesis and stomatal conductance in 'Vermentino' (Table 5), which was similar to that of well-watered plants. Pn and Gs significantly decreased only under severe water deficit RDI-2 or in the absence of irrigation. At Usini, in both 'Cabernet Sauvignon' and 'Cagnulari', Pn and Gs were the highest in well-watered plants and the lowest in the dry treatment, but the differences were not significant between the wet and RDI-1 treatments. While "Cabernet Sauvignon" and "Cagnulari" plants had similar photosynthetic activity, the Pn in 'Vermentino' was almost 1/3 of that of the other cultivars.

Table 5. Net photosynthetic rate (Pn), stomatal conductance (Gs), maximum quantum efficiency of PSII photochemistry (Fv/Fm), maximum photochemical efficiency of photosystem II in the light (Fv'/Fm'), actual photochemical efficiency of PSII (ΦPSII) and non-photochemical quenching (NPQ) in selected fully-developed leaves of 'Vermentino', 'Cabernet' and 'Cagnulari' in response to well-watered conditions (wet), moderate (RDI-1), severe (RDI-2) water deficit and dry conditions (dry). Values represent the mean ± SE. Different letters indicate significant differences between treatments ($p \leq 0.05$) based on one-way ANOVA (Tukey test).

				'Vermentino'		
	Pn	**Gs**	**Fv/Fm**	**Fv'/Fm'**	**ΦPSII**	**NPQ**
	μmol m^{-2} s^{-1}	mmol m^{-2} s^{-1}				
Wet	6.5 ± 0.3 a	0.27 ± 0.04 a	0.8 ± 0.01 a	0.4 ± 0.01 a	0.2 ± 0.03 a	2.1 ± 0.2 b
RDI-1	6.3 ± 0.7 a	0.26 ± 0.04 a	0.8 ± 0.01 a	0.4 ± 0.01 a	0.2 ± 0.02 a	2.2 ± 0.2 b
RDI-2	2.5 ± 0.5 b	0.07 ± 0.02 b	0.8 ± 0.01 a	0.3 ± 0.02 b	0.1 ± 0.01 b	3.1 ± 0.2 a
Dry	2.6 ± 0.7 b	0.06 ± 0.01 b	0.8 ± 0.01 a	0.4 ± 0.02 b	0.1 ± 0.01 b	2.8 ± 0.2 a
				'Cabernet'		
	Pn	**Gs**	**Fv/Fm**	**Fv'/Fm'**	**ΦPSII**	**NPQ**
	μmol m^{-2} s^{-1}	mmol m^{-2} s^{-1}				
Wet	15.9 ± 1.1 a	0.39 ± 0.09 a	0.8 ± 0.01 a	0.3 ± 0.01 a	0.1 ± 0.01 a	2.2 ± 0.01a
RDI-1	13.0 ± 0.9 ab	0.32 ± 0.07 ab	0.8 ± 0.01 a	0.4 ± 0.02 a	0.1 ± 0.03 ab	2.3 ± 0.02 ab
RDI-2	10.1 ± 2.6 b	0.17 ± 0.05 ab	0.8 ± 0.01 a	0.4 ± 0.02 a	0.1 ± 0.03 ab	2.0 ± 0.02 ab
Dry	5.8 ± 1.5 b	0.12 ± 0.03 b	0.8 ± 0.01 a	0.3 ± 0.02 b	0.1 ± 0.01 b	2.6 ± 0.02 b
				'Cagnulari'		
	Pn	**Gs**	**Fv/Fm**	**Fv'/Fm'**	**ΦPSII**	**NPQ**
	μmol m^{-2} s^{-1}	mmol m^{-2} s^{-1}				
Wet	14.7 ± 1.3 a	0.35 ± 0.05 a	0.8 ± 0.01 a	0.4 ± 0.02 a	0.1 ± 0.02 a	1.8 ± 0.2 b
RDI-1	12.1 ± 0.9 ab	0.28 ± 0.04 ab	0.8 ± 0.01 a	0.4 ± 0.04 a	0.1 ± 0.03 a	2.0 ± 0.3 a
RDI-2	9.2 ± 1.1 b	0.17 ± 0.05 bc	0.8 ± 0.01 a	0.4 ± 0.03 a	0.1 ± 0.01 a	2.0 ± 0.2 a
Dry	5.3 ± 0.2 b	0.12 ± 0.03 c	0.8 ± 0.01 a	0.4 ± 0.02 b	0.1 ± 0.02 b	2.5 ± 0.3 a

The maximum photochemical efficiency of PSII in dark adapted leaves was not affected by water status in any of the tested cultivars (Table 5). The maximum efficiency of PSII photochemistry in light-adapted leaves, Fv'/Fm' was significantly lower at the severe water deficit RDI-2 and in the dry condition in 'Vermentino' and only in the dry condition in 'Cabernet Sauvignon' and 'Cagnulari'. The effective photochemical quantum yield of PSII, Φ_{PSII} of 'Vermentino', was significantly reduced

only in RDI-2 and dry (40–50% of reduction, respectively). The non-photochemical quenching (NPQ) significantly increased only in response to RDI-2 and dry water deficit treatment by 20–30%, respectively. In both 'Cabernet Sauvignon' and 'Cagnulari', the water limitation significantly decreased Φ_{PSII} only in the dry status (36% and 33%, respectively), while NPQ significantly increased (15% and 29%, respectively).

The high spatial resolution obtained in the thermal imagery enabled the identification of single vines, allowing a comparison between data extracted from the CWSI map and physiological measurements. The analysis of remote and physiological data from the CWSI map was performed by means of the average values contained in the ROI polygons along the row axes, centred on each referenced sample vine, using the second data extraction method described in the Material and Methods section. The results of the correlation between the average data extracted from the CWSI map and the physiological measurements for each vineyard are given in Table 6. Data analysis showed a positive correlation between the CWSI and leaf temperatures and a negative correlation with Pn in all cultivars. Furthermore, all cultivars presented a positive correlation with the NPQ index and a negative correlation with Fv'/Fm'. These correlations corroborate our results, indicating a decrease in Φ_{PSII} and the concomitant increase in NPQ.

Table 6. Pearson correlation value and associated pairwise two-sided p-values between CWSI data and physiological measurements related to sample vines. CTleaf: leaf canopy temperature measured at the ground; Fv'/Fm': maximum photochemical efficiency of photosystem II in the light; NPQ: non-photochemical quenching; Φ_{PSII}: actual photochemical efficiency of photosystem II; Pn: net photosynthesis.

Cultivars	CTleaf	Fv'/Fm'	NPQ	Φ_{PSII}	Pn
'Vermentino'	0.49 ***	−0.43 **	0.47 **	−0.35 *	−0.55 ***
'Cabernet'	0.75 ****	−0.37 *	0.27 ns	−0.16 ns	−0.66 ***
'Cagnulari'	0.63 ***	−0.48 *	0.09 ns	−0.49 *	−0.80 ****

Significance codes for pairwise two-sided *p*-values: **** $p = 0$; *** $p = 0.001$; ** $p = 0.01$; * $p = 0.05$; ns > 0.05.

4. Discussion

Regarding the remote sensing dataset, the different CWSI absolute values observed at the two vineyards reflected weather conditions observed during the day of the flights. In particular, at Arzachena, 'Vermentino' vines were experiencing extreme air temperatures (daily maximum and average values of about 37 °C and 27 °C, respectively), very low daily minimum relative humidity values (28% in average) and, consequently, very high mean values of vapor pressure deficit (4.15 kPa). At Usini, the weather conditions were cooler and wetter compared to Arzachena, with approximately 4 °C lower daily maximum and mean temperatures, and 10% higher daily minimum relative humidity. These environmental conditions had a relevant impact on the canopy temperature and plant stress status, as clearly indicated by the higher mean CWSI values measured at Arzachena. Just as expected, at both sites the CWSI values increased moving from the wet to the dry treatment and the CWSI spatial pattern reflected the irrigation regimes very well. The only exception was observed at Arzachena over 'Vermentino', where RDI-1 treatment showed an average CWSI value (0.72) slightly lower than wet treatment (0.79). This may be attributed to the complex orography of the Arzachena vineyard, where the elevation of the western portion of the field is higher than the eastern part, with an average slope of approximately 10%. At the Arzachena vineyard, the effect of the slope may have led to a water dispersion from the wet experimental plot to the RDI-1 plot. The slope of a vineyard can be a key factor in soil water dynamics and may limit the effect of irrigation regimes by altering the amount of water that remains in the soil and, consequently, the amount of water available for plants. Recent studies discussed and quantified the significant effects of the slope in the flow rate distribution under drip irrigation conditions, highlighting that, under moderate slope conditions (around 5–10%), elevation information is crucial to identifying the spatial structure of water distribution throughout the field [38].

Proximal sensing datasets indicate that CWSI robustness was much more influenced by environmental conditions rather than by the grapevine genotypes under study, confirming that in Mediterranean areas CWSI is a reliable indicator of crop-water status, independent of the cultivars [39]. Focusing on the UAV flight days, proximal thermal data were in line with remote sensed data at both sites (Figure 2d,e). In addition, the CWSI values were consistent with those reported by other authors [15] for moderately stressed 'Pinot noir' vines (ranging between 0.3 and 0.5), and severely stressed vines (equal to or above 0.7).

The drought effects on grapevine photosynthesis are widely known because this species is very sensitive to environmental stresses, including water availability, temperature and CO_2 [22,40]. In this study, we found that water deficit induced the inhibition of photosynthesis caused by decreases in stomatal conductance, as clearly observed also by Flexas [41–43]. All the tested cultivars activated effective photoprotective mechanisms when drought induced photosynthesis inhibition. In fact, the photochemical efficiency of PSII measured after the darkening period (Fv/Fm) remained almost constantly close to 0.8, the maximum value recorded under optimal environmental conditions for most plant species [44–46]. Signs of photoinhibition can be observed when Fv/Fm declines and thus a decrease of the photochemical efficiency of PSII, called the 'down-regulation of photochemistry', occurs, revealing permanent photoinhibition [47–49]. Furthermore, the increase in NPQ provides protection against damage by excessive energy, in agreement with previous studies on grapes [40], pepper [50] and Amur grapes (Vitis Amurensis Rupr.) [51]. In fact, under environmental stresses such as drought, plants can divert absorbed light from photochemistry to other processes, thereby protecting the leaves from light-induced damage [26].

The thermal monitoring of vegetation is a function of the energy balance of different combinations of grapevine, other vegetation and bare soil, between the rows of grapevines. A key factor is related to natural environments where leaf temperatures fluctuate rapidly as radiation, wind speed and air temperatures vary. In our experimental vineyards, these assumptions are more evident due to the relatively low cover fractions (20–28%). However, the use of thermal imaging methodologies is now largely considered to be the best compromise for canopy instantaneous measurement, preventing errors due to rapid microclimatic variations. Moreover, in our work the high spatial resolution (less than 10 cm) allowed pure canopy pixel extraction, removing underlying shadows and soil pixels. From this point of view, the cover fraction of the grapevine in the experimental sites should not greatly affect the accuracy of temperature measurements. Another critical aspect is the procedure for estimating reference temperatures (Tdry and Twet), which is crucial for obtaining accurate crop water stress maps. The theoretical approach requires knowledge of crop resistance properties and net radiation, in addition to measured (Tc−Ta) and vapour pressure deficit (VPD), which makes it difficult to apply this method in practice. The empirical approach is based on relating canopy-air temperature difference to VPD [29]. Another method is based on the energy balance equation and requires an estimation of net radiation and an aerodynamic resistance factor. Other approaches are based on using natural and artificial wet and dry reference surfaces. The use of wetted or petroleum-jelly-covered leaves [52] can largely overcome problems of ensuring equivalent radiative properties with respect to artificial surfaces, but remains the problem of ensuring that all leaves are similarly exposed to the sun. In our study, five young, fully-expanded leaves with the same exposure, were chosen. Jones [30] concluded that real leaves, either sprayed with water or covered in petroleum jelly to stop transpiration, provided the best reference because of the similar radiometric and aerodynamic properties compared to the canopy being studied. Another source of uncertainties could be related to the erroneous consideration of CWSI as the entire season water stress index. CWSI measured on a single day did not provide a good estimation of the variations of plant water status [53]. The objective of the work was to evaluate the instantaneous correspondence between water status characterizations through different sensing techniques.

The technique applied in the present study builds on use of the CWSI, which has been tested in a number of studies, using ground and satellite data. The UAV instrumentation has previously been

tested to derive drought stress in agricultural crops such as barley [54], olive [4,5], and fruit species [16]. UAV was also applied to study vegetation index linkages to water stress in grapevines [55] but not yet to investigate CWSI in a grapevine crop, as done in the present research and other studies [14,15].

5. Conclusions

The relationship between the crop water stress index (CWSI) and vine water status confirmed the capacity of thermal remote sensing to assess vineyard water status. Thermal remote sensing can detect the spatial variability in water status, without the need to install an unreasonable number of on-site sensors in the vineyard. Thermal imagery can also assist in making decisions concerning irrigation management in precision agriculture. The use of CWSI maps gives the main advantage of managing irrigation at a large scale, taking into account the spatial variability of vine water status and developing an approach for providing precision irrigation recommendations. For practical purposes, it would be necessary to replicate the measurements on several dates during the summer to assess their consistency.

Thermal measurements from proximal sensing have been demonstrated to be able to well-differentiate different regimes in water management, confirming the good performance of this technique. The differences in CWSI values between moderate or severe water deficit treatments (RDI-1 and RDI-2) were in almost all cases (sites and varieties) statistically significant. The differences between treatments in the CWSI results obtained from remote sensing were consistent with both proximal sensing and physiological measurements.

Considering the two autochthonous cultivars located in the two different sites ('Vermentino' in Arzachena and 'Cagnulari' inUsini), our results highlighted a different percentage increment between RDI-1 and RDI-2 treatments. 'Vermentino' reported 25%, 32%, 60% and 73% increment for CWSI, SWP, Pn and Gs, respectively, while 'Cagnulari' 18%, 59%, 23% and 39% increment for the same variables. 'Vermentino' showed a higher percentage increment than 'Cagnulari' for all variables except for SWP. The UAV system used in this work has previously been tested in different crops, with only little experience with grapevines. However, our experiment, due to a spatial resolution better than 0.10 m pixel^{-1}, is unique since the methodology allowed us to obtain an extreme accuracy of pure canopy pixel extraction in vineyards located at different sites and over different cultivars.

In summary, the results confirmed that also for Mediterranean sites and different grapevine cultivars, thermal indices, such as CWSI and the linear thermal index, are likely to be very representative of the variations in photosynthesis, stomatal conductance and light use efficiency of photosystem II. Consequently, they can be used to advise the implementation of precision irrigation scheduling according to the specific physiological status of grapevines.

Future work will be necessary to acquire thermal images on several dates leading to a quantitative method suitable for assisting irrigation management decisions.

Acknowledgments: This research was supported by the Italian MIUR (Progetto Premiale AQUA to CNR). The authors would like to thank AGRIS Sardinia for the ground measurements, Sa Tanca e su Re (Usini) and Vigne Surrau (Arzachena) farms for experimental vineyards, Sigma Ingegneria and Skorpion Engineering for technological contribution in the UAV platform development.

Author Contributions: Alessandro Matese, Rita Baraldi, Carla Cesaraccio and Massimiliano Giuseppe Mameli conceived and designed the experiments. All authors were involved in the field campaign measurements. Alessandro Matese, Rita Baraldi, Carla Cesaraccio, Pierpaolo Duce Osvaldo Facini and Alessandra Piga wrote the manuscript. Rita Baraldi and Osvaldo Facini performed the statistical data analysis, supported by Carla Cesaraccio, Salvatore Filippo Di Gennaro, Pierpaolo Duce, and Alessandra Piga. Andrea Berton performed the UAV flights and wrote the technical sections of the manuscript. Massimiliano Giuseppe Mameli and Alessandro Zaldei supported development and measurements.

Conflicts of Interest: The authors declare no conflict of interest.

References

1. Ojeda, H.; Andary, C.; Kraeva, E.; Carbonneau, A.; Deloire, A. Influence of pre- and post-veraison water deficit on synthesis and concentration of skin phenolic compounds during berry growth of Vitis vinifera cv Shiraz. *Am. J. Enol. Viticult.* **2002**, *53*, 261–267.
2. Jackson, R.D.; Idso, S.B.; Reginato, R.J.; Pinter, P.J. Canopy temperature as a crop water stress indicator. *Water Resour. Res.* **1981**, *17*, 1133–1138. [CrossRef]
3. Jones, H.G. Irrigation scheduling: Advantages and pitfalls of plant-based methods. *J. Exp. Bot.* **2004**, *55*, 2427–2436. [CrossRef] [PubMed]
4. Berni, J.A.J.; Zarco-Tejada, P.J.; Sepulcre-Canto, G.; Fereres, E.; Villalobos, F. Mapping canopy conductance and CWSI in olive orchards using high resolution thermal remote sensing imagery. *Remote Sens. Environ.* **2009**, *113*, 2380–2388. [CrossRef]
5. Berni, J.A.J.; Zarco-Tejada, P.J.; Suarez, L.; Fereres, E. Thermal and narrowband multispectral remote sensing for vegetation monitoring from an unmanned aerial vehicle. *IEEE Trans. Geosci. Remote Sens.* **2009**, *47*, 722–738. [CrossRef]
6. Gonzalez-Dugo, V.; Zarco-Tejada, P.; Berni, J.A.J.; Suarez, L.; Goldhamer, D.; Fereres, E. Almond tree canopy temperature reveals intra-crown variability that is water stress-dependent. *Agric. For. Meteorol.* **2012**, *154–155*, 156–165. [CrossRef]
7. Zarco-Tejada, P.J.; Gonzalez-Dugo, V.; Berni, J.A.J. Fluorescence, temperature and narrow-band indices acquired from a UAV platform for water stress detection using a micro-hyperspectral imager and a thermal camera. *Remote Sens. Environ.* **2012**, *117*, 322–337. [CrossRef]
8. Grant, O.M.; Tronina, L.; Jones, H.G.; Chaves, M.M. Exploring thermal imaging variables for the detection of stress responses in grapevine under different irrigation regimes. *J. Exp. Bot.* **2007**, *58*, 815–825. [CrossRef] [PubMed]
9. Möller, M.; Alchanatis, V.; Cohen, Y.; Meron, M.; Tsipris, J.; Naor, A.; Ostrovsky, V.; Sprintsin, M.; Cohen, S. Use of thermal and visible imagery for estimating crop water status of irrigated grapevine. *J. Exp. Bot.* **2007**, *58*, 827–838. [CrossRef] [PubMed]
10. Gontia, N.K.; Tiwari, K.N. Development of crop water stress index of wheat crop for scheduling irrigation using infrared thermometry. *Agric. Water Manag.* **2008**, *95*, 1144–1152. [CrossRef]
11. Jones, H.G.; Serraj, R.; Loveys, B.R.; Xiong, L.; Wheaton, A.; Price, A.H. Thermal infrared imaging of crop canopies for the remote diagnosis and quantification of plant responses to water stress in the field. *Funct. Plant Biol.* **2009**, *36*, 978–979. [CrossRef]
12. Romano, G.; Zia, S.; Spreer, W.; Sanchez, C.; Cairns, J.; Araus, J.L.; Müller, J. Use of thermography for high throughput phenotyping of tropical maize adaptation in water stress. *Comput. Electron. Agric.* **2011**, *79*, 67–74. [CrossRef]
13. Alchanatis, V.; Cohen, Y.; Cohen, S.; Moller, M.; Sprinstin, M.; Meron, M.; Tsipris, J.; Saranga, Y.; Sela, E. Evaluation of different approaches for estimating and mapping crop water status in cotton with thermal imaging. *Precis. Agric.* **2010**, *11*, 27–41. [CrossRef]
14. Baluja, J.; Diago, M.P.; Balda, P.; Zorer, R.; Meggio, F.; Morales, F.; Tardaguila, J. Assessment of vineyard water status variability by thermal and multispectral imagery using an unmanned aerial vehicle (UAV). *Irrig. Sci.* **2012**, *30*, 511–522. [CrossRef]
15. Bellvert, J.; Zarco-Tejada, P.J.; Girona, J.; Fereres, E. Mapping crop water stress index in a 'Pinot-noir' vineyard: Comparing ground measurements with thermal remote sensing imagery from an unmanned aerial vehicle. *Precis. Agric.* **2014**, *15*, 361–376. [CrossRef]
16. Gonzalez-Dugo, V.; Zarco-Tejada, P.; Nicolas, E.; Nortes, P.A.; Alarcon, J.J.; Intrigliolo, D.S.; Fereres, E. Using high resolution UAV thermal imagery to assess the variability in the water status of five fruit tree species within a commercial orchard. *Precis. Agric.* **2013**, *14*, 660–678. [CrossRef]
17. Humplík, J.F.; Lazár, D.; Husičková, A.; Spíchal, L. Automated phenotyping of plant shoots using imaging methods for analysis of plant stress responses—A review. *Plant Methods* **2015**, *11*, 29. [CrossRef] [PubMed]
18. Nilsson, H.E. Remote sensing and image analysis in plant pathology. *Annu. Rev. Phytopathol.* **1995**, *15*, 489–527. [CrossRef] [PubMed]
19. Peñuelas, J.; Filella, I. Visible and near-infrared reflectance techniques for diagnosing plant physiological status. *Trends Plant Sci.* **1998**, *3*, 151–156. [CrossRef]

20. Lichtenthaler, H.K.; Miehé, J.A. Fluorescence imaging as a diagnostic tool for plant stress. *Trends Plant Sci.* **1997**, *2*, 316–320. [CrossRef]
21. Riccardi, M.; Mele, G.; Pulvento, C.; Lavini, A.; d'Andria, R.; Jacobsen, S.E. Non-destructive evaluation of chlorophyll content in quinoa and amaranth leaves by simple and multiple regression analysis of RGB image components. *Photosynth. Res.* **2014**, *120*, 263–272. [CrossRef] [PubMed]
22. Salazar-Parra, C.; Aguirreolea, J.; Sànchez-Dìaz, M.; Irigoyen, J.J.; Morales, F. Photosynthetic response of Tempranillo grapevine to climate change scenarios. *Ann. Appl. Biol.* **2012**, *161*, 277–292. [CrossRef]
23. Demmig-Adams, B.; Adams, W.W., III; Barker, D.H.; Logan, B.A.; Bowling, D.R.; Verhoeven, A.S. Using chlorophyll fluorescence to assess the fraction of absorbed light allocated to thermal dissipation of excess excitation. *Physiol. Plant.* **1996**, *98*, 253–264. [CrossRef]
24. Baker, N.R.; Rosenqvist, E. Applications of chlorophyll fluorescence can improve crop production strategies: An examination of future possibilities. *J. Exp. Bot.* **2004**, *55*, 1607–1621. [CrossRef] [PubMed]
25. Borawska-Jarmułowicz, B.; Mastalerczuk, G.; Pietkiewicz, S.; Kalaji, M.H. Low temperature and hardening effects on photosynthetic apparatus efficiency and survival of forage grass varieties. *Plant Soil Environ.* **2014**, *60*, 177–183.
26. Maxwell, K.; Johnson, G.N. Chlorophyll fluorescence—A practical guide. *J. Exp. Bot.* **2000**, *51*, 659–668. [CrossRef] [PubMed]
27. Kalaji, H.M.; Schansker, G.; Ladle, R.J.; Goltsev, V.; Bosa, K.; Allakhverdiev, S.I.; Brestic, M.; Bussotti, F.; Calatayud, A.; Dąbrowski, P.; et al. Frequently asked questions about in vivo chlorophyll fluorescence: Practical issues. *Photosynth. Res.* **2014**, *121*, 122–158. [CrossRef] [PubMed]
28. Jones, H.G.; Vaughan, R.A. *Remote Sensing of Vegetation: Principles, Techniques, and Applications*; Oxford University Press: Oxford, UK, 2010; ISBN 9780199207794.
29. Idso, S.B.; Jackson, R.D.; Pinter, P.J.; Reginato, R.J.; Hatfield, J.L. Normalizing the stress degree day parameter for environmental variability. *Agric. Meteorol.* **1981**, *24*, 45–55. [CrossRef]
30. Jones, H.G.; Stoll, M.; Santos, T.; de Sousa, C.; Chaves, M.M.; Grant, O.M. Use of infrared thermography for monitoring stomatal closure in the field: Application to grapevine. *J. Exp. Bot.* **2002**, *53*, 2249–2260. [CrossRef] [PubMed]
31. Matese, A.; Di Gennaro, S.F.; Berton, A. Assessment of a canopy height model (CHM) in a vineyard using UAV-based multispectral imaging. *Int. J. Remote Sens.* **2017**, *38*, 2150–2160. [CrossRef]
32. Leinonen, I.; Jones, H.G. Combining thermal and visible imagery for estimating canopy temperature and identifying plant stress. *J. Exp. Bot.* **2004**, *55*, 1423–1431. [CrossRef] [PubMed]
33. Costa, J.M.; Ortuño, M.F.; Lopes, C.M.; Chaves, M.M. Grapevine varieties exhibiting differences in stomatal response to water deficit. *Funct. Plant Biol.* **2012**, *39*, 179–189. [CrossRef]
34. Pou, A.; Diago, M.P.; Medrano, H.; Baluja, J.; Tardaguila, J. Validation of thermal indices for water stress status identification in grapevine. *Agric. Water Manag.* **2014**, *134*, 60–72. [CrossRef]
35. Loveys, B.R.; Jones, H.G.; Theobald, J.C.; McCarthy, M.G. An assessment of plant-based measures of grapevine performance as irrigation-scheduling tools. *Acta Hortic.* **2008**, *792*, 391–403. [CrossRef]
36. Van Kooten, O.; Snel, J.F. The use of chlorophyll fluorescence nomenclature in plant stress physiology. *Photosynth. Res.* **1990**, *25*, 147–150. [CrossRef] [PubMed]
37. Giorio, P. Black leaf-clips increased minimum fluorescence emission in clipped leaves exposed to high solar radiation during dark adaptation. *Photosynthetica* **2011**, *49*, 371–379. [CrossRef]
38. Tisseyre, B.; Ducanchez, A. Spatial variability of drip irrigation in small vine fields of south of France. In *Precision Agriculture '13*; Stafford, J.V., Ed.; Wageningen Academic Publishers: Wageningen, The Netherlands, 2013; pp. 251–257.
39. García-Tejero, I.F.; Costa, J.M.; Egipto, R.; Durán-Zuazo, V.H.; Lima, R.S.N.; Lopes, C.M.; Chaves, M.M. Thermal data to monitor crop-water status in irrigated Mediterranean viticulture. *Agric. Water Manag.* **2016**, *176*, 80–90. [CrossRef]
40. Wang, Z.Z.; Zheng, P.; Meng, J.F.; Xi, Z.M. Effect of exogenous 24-epibrassinolide on chlorophyll fluorescence, leaf surface morphology and cellular ultrastructure of grape seedlings (*Vitis vinifera* L.) under water stress. *Acta Physiol. Plant.* **2015**, *37*, 1729–1740. [CrossRef]
41. Flexas, J.; Bota, J.; Escalona, J.M.; Sampol, B.; Medrano, H. Effects of drought on photosynthesis in grapevines under field conditions: An evaluation of stomatal and mesophyll limitations. *Funct. Plant Biol.* **2002**, *29*, 461–471. [CrossRef]

42. Flexas, J.; Escalona, J.M.; Medrano, H. Down-regulation of photosynthesis by drought under field conditions in grapevine leaves. *Aust. J. Plant Physiol.* **1998**, *25*, 892–900. [CrossRef]
43. Flexas, J.; Ribas-Carbò, M.; Dìaz-Espejo, A.; Galmès, J.; Medrano, H. Mesophyll conductance to CO_2: Current knowledge and future prospects. *Plant Cell Environ.* **2008**, *31*, 602–621. [CrossRef] [PubMed]
44. Björkman, O.; Demmig, B. Photon yield of O_2 evolution and chlorophyll fluorescence characteristics of 77K among vascular plants of diverse origins. *Planta* **1987**, *170*, 489–504. [CrossRef] [PubMed]
45. Morales, F.; Abadía, A.; Abadía, J. Chlorophyll fluorescence and photon yield of oxygen evolution in iron-deficient sugar beet (*Beta vulgaris* L.) leaves. *Plant Physiol.* **1991**, *97*, 866–893. [CrossRef]
46. Ripullone, F.; Rivelli, A.R.; Baraldi, R.; Guarini, R.; Guerrieri, R.; Magnani, F.; Peñuelas, J.; Raddi, S.; Borghetti, M. Effectiveness of the photochemical reflectance index to track photosynthetic activity over a range of forest tree species and plant water status. *Funct. Plant Biol.* **2011**, *38*, 177–186. [CrossRef]
47. Morales, F.; Abadìa, A.; Abadìa, J. Photoinhibition and photoprotection under nutrient deficiencies, drought and salinity. In *Photoprotection, Photoinhibition, Gene Regulation and Environment*; Demming-Adams, B., Adams, W.W., III, Mattoo, A.K., Eds.; Springer: Dordrecht, The Netherlands, 2006; pp. 65–85.
48. Grant, O.M.; Tronina, L.; Ramalho, J.C.; Besson, C.K.; Lobo-Do-Vale, R.; Pereira, J.S.; Jones, H.G.; Chaves, M.M. The impact of drought on leaf physiology of *Quercus suber* L. trees: Comparison of an extreme drought event with chronic rainfall reduction. *J. Exp. Bot.* **2010**, *61*, 4361–4371. [CrossRef] [PubMed]
49. Pascual, I.; Azcona, I.; Morales, F.; Aguirreole, J.; Sànchez-Dìaz, M. Photosynthetic response of pepper plants to wilt induced by Verticillium dahliae and soil water deficit. *J. Plant Physiol.* **2010**, *167*, 701–708. [CrossRef] [PubMed]
50. Hu, W.H.; Yan, X.H.; Xiao, Y.A.; Zeng, J.J.; Qi, H.J.; Ogweno, J.O. 24-Epibrassinosteroid alleviate drought-induced inhibition of photosynthesis in Capsicum annuum. *Sci. Hortic.* **2013**, *150*, 232–237. [CrossRef]
51. Qin, H.Y.; Ai, J.; Xu, P.L.; Wang, Z.X.; Zhao, Y.; Yang, Y.M.; Fan, S.T.; Shen, Y.J. Chlorophyll fluorescence parameters and ultrastructure in amur grape (*Vitis amurensis* Rupr.) under salt stress. *Acta Bot. Boreal. Occident. Sin.* **2013**, *33*, 1159–1164.
52. Jones, H.G. Use of infrared thermometry for estimation of stomatal conductance in irrigation scheduling. *Agric. For. Meteorol.* **1999**, *95*, 139–149. [CrossRef]
53. Santesteban, L.; Di Gennaro, S.; Herrero-Langreo, A.; Miranda, C.; Royo, J.; Matese, A. High-resolution uav-based thermal imaging to estimate the instantaneous and seasonal variability of plant water status within a vineyard. *Agric. Water Manag.* **2017**, *183*, 49–59. [CrossRef]
54. Hoffmann, H.; Jensen, R.; Thomsen, A.; Nieto, H.; Rasmussen, J.; Friborg, T. Crop water stress maps for an entire growing season from visible and thermal UAV imagery. *Biogeosciences* **2016**, *13*, 6545–6563. [CrossRef]
55. Espinoza, C.Z.; Khot, L.R.; Sankaran, S.; Jacoby, P.W. High Resolution Multispectral and Thermal Remote Sensing-Based Water Stress Assessment in Subsurface Irrigated Grapevines. *Remote Sens.* **2017**, *9*, 961. [CrossRef]